Analyst

PAPER

View Article Online
View Journal | View Issue

Cite this: *Analyst*, 2016, **141**, 4432

Sensing hydrocarbons with interband cascade lasers and substrate-integrated hollow waveguides

Igor José Gomes da Silva,[a,b] Erhan Tütüncü,[b] Markus Nägele,[c] Peter Fuchs,[d] Marc Fischer,[d] Ivo M. Raimundo, Jr[a] and Boris Mizaikoff*[b]

Received 22nd March 2016,
Accepted 4th May 2016

DOI: 10.1039/c6an00679e

www.rsc.org/analyst

Tunable diode laser absorption spectroscopy (TDLAS) is an excellent analytical technique for gas sensing applications. *In situ* sensing of relevant hydrocarbon gases is of substantial interest for a variety of in-field scenarios including environmental monitoring and process analysis, ideally providing accurate, molecule specific, and rapid information with minimal sampling requirements. Substrate-integrated hollow waveguides (iHWGs) have demonstrated superior properties for gas sensing applications owing to minimal sample volumes required while simultaneously serving as efficient photon conduits. Interband cascade lasers (ICLs) are recently emerging as mid-infrared light sources operating at room temperature, with low power consumption, and providing excellent potential for integration. Thereby, portable and handheld mid-infrared sensing devices are facilitated. Methane (CH_4) is among the most frequently occurring, and thus, highly relevant hydrocarbons requiring *in situ* emission monitoring by taking advantage of its distinct molecular absorption around 3 μm. Here, an efficient combination of iHWGs with ICLs is presented providing a methane sensor calibrated in the range of 100 to 2000 ppm_v with a limit of detection at 38 ppm_v at the current stage of development. Furthermore, a measurement precision of 0.62 ppb_v during only 1 s of averaging time has been demonstrated, thereby rendering this sensor concept useful for in-line and on-site emission monitoring and process control applications.

Introduction

Atmospheric methane (CH_4) is an important anthropogenic greenhouse gas next to carbon dioxide and water, and plays an important role in tropospheric chemistry, as well as stratospheric ozone chemistry. Atmospheric methane is a colorless and odorless gas widely distributed in nature, therefore frequently occurring as a mixture of both natural (*e.g.*, from wetlands, sea surfaces, *etc.*) and anthropogenic sources (*e.g.*, agriculture, fossil fuel drilling and mining, shale gas mining, *etc.*). While continuously assessing the global and seasonal distribution of CH_4 over extended time periods may facilitate narrowing down the location of major emission sources, pinpointing and identification of the type of source are exceedingly difficult.[1,2]

The main health hazard associated with methane gas results from its combustibility, as mixtures of 5 to 15% methane in air are highly explosive. Moreover, high concentrations of methane in confined areas may lead to asphyxia resulting from a decrease in available oxygen. Potential effects of oxygen deficiency are headaches, nausea, dizziness, and unconsciousness.[1,3]

Considering currently available data, methane does not appear to have any long-term or chronic health effects. While the National Institute for Occupational Safety and Health does not list any effects of long-term or repeated exposure to methane, it clearly states that no information on its potential to cause cancer or birth defects is available. Likewise, no Occupational Safety and Health Administration (OSHA) standards or regulations are listed regarding methane exposure. However, extended research may be needed to understand any long-term effects of methane exposure in depth, in particular since an increase in methane release *e.g.*, *via* mining of gas-containing mineral shales near populated areas is anticipated.[3]

Optical methods based on infrared laser spectroscopy are suitable analytical platforms for direct methane sensing,[4–9] as they usually do not require extensive gas sample pretreatment unlike conventional methods such as mass spectrometry or gas chromatography. In addition, optical methods provide fast response times, on-line and in-line measurement capabilities, and facilitate remote sensing.[10]

Consequently, spectroscopic and optical sensing schemes are progressively more applied for industrial process control,

[a]*Institute of Chemistry, State University of Campinas - UNICAMP, 13083-970 Campinas, Brazil*
[b]*Institute of Analytical and Bioanalytical Chemistry, Ulm University, 89081 Ulm, Germany. E-mail: boris.mizaikoff@uni-ulm.de*
[c]*OptoPrecision GmbH, 28357 Bremen, Germany*
[d]*Nanoplus GmbH, 97218 Gerbrunn, Germany*

monitoring of health-relevant or safety-relevant gas concentrations in workplace scenarios, and in environmental and atmospheric gas tracing just to name a few. Among these techniques, tunable diode laser absorption spectroscopy (TDLAS) is increasingly adopted for such applications.[10]

Compared to other sensing techniques, TDLAS is a particularly robust method providing accurate and reliable analytical results. In particular, using single-mode semiconductor laser light sources, which can be tuned – by current or temperature – to the desired absorption line, gaseous species may nowadays be selectively sensed in or close to real time at sensitivities reaching parts-per-million (ppm_v) to parts-per-trillion (ppt_v) concentration levels. Hence, the prolific nature of this research field is immediately evident.[11]

Major improvements in selectivity during TDLAS measurement – and in particular for sensing hydrocarbons – rely on addressing particularly pronounced absorption bands associated with the constituents of interest. For most industrially and environmentally relevant species, these signatures are most distinctive and discriminative in the mid-infrared (MIR) wavelength band (*i.e.*, 3–15 μm). In this spectral regime, the absorption intensities are orders of magnitude higher compared to the near-infrared (NIR) and other potentially useful spectral regions.[12] Likewise, the most pronounced absorptions of methane similar to carbon dioxide, nitric oxide, water, and other hydrocarbons are located in the MIR window.[13,14] However, efficient TDLAS sensing schemes require single-mode laser sources emitting in continuous wave (CW) operation in the 3–15 μm spectral range at reasonable power consumption and optical output power, and at ambient temperature. In particular, owing to the lack of suitable laser diodes in the 3–6 μm regime for sensing hydrocarbons this wavelength range was referred to as the 'gap in spectroscopic gas sensing'.[15,16]

With the advent of compact MIR laser light sources including quantum cascade lasers (QCLs), and – more recently – interband cascade lasers (ICLs), the development of an advanced generation of optical gas sensing devices combining the advantages of TDLAS with the discriminatory and pronounced molecular signatures in the MIR has been realised.[17] Combined with innovative waveguide technologies such as substrate-integrated hollow waveguides (iHWGs) providing light-guiding channels integrated into a solid-state substrate while simultaneously acting as a highly miniaturized gas absorption cell, superior performance for a wide range of gas sensing scenarios may be anticipated.[18]

Methane (CH_4) is among the most relevant gases for *in situ* emission monitoring applications providing a distinct absorption signature at 3.368–3.370 μm. While in this wavelength regime nowadays both QCLs and ICLs are available, the superior thermal characteristics, the low power consumption, and the high level of integration favor ICLs for portable and handheld hydrocarbon sensing devices.[19–21]

In this study, we present first quantitative measurements of methane performed *via* the combination of a distributed feedback (DFB) ICL with an iHWG establishing the prototype of a methane sensor useful for emission monitoring and process control applications.

Experimental

Methane absorption in the mid-infrared

The strongest discriminatory absorption lines of methane are located in the rotational–vibrational band ranging from 3.1 to 3.5 μm. More specifically, ICLs available to this study provided spectral access to the region 3.363–3.370 μm. The calculated absorbance for 100 ppm_v methane under atmospheric conditions (*i.e.*, 1013 hPa, 296 K) is shown in Fig. 1 using the HITRAN database.[21]

Distributed feedback interband cascade laser

The DFB-ICL used in this study utilizes lateral metal gratings ensuring DFB behavior, and was fabricated *via* type-II W-shaped semiconductor quantum wells (QW).[22] The gratings with dimensions on the order of 100 nm were defined next to the sidewalls of the etched ridge waveguide structure *via* electron beam lithography. The feedback structures were then patterned by metal evaporation, thereby resulting in the desired DFB-ICL devices.[16] The laser emission is centered at around 3.366 μm, and exhibits a spectral line width <10 MHz with a side-mode suppression ratio exceeding 32 dB.

The operating parameters of this DFB-ICL comprise a current of 35 mA, a voltage of 3.8 V, and an operation temperature of 25 °C. Similar to lasers based on ternary and quaternary semiconductors, the spectral emission of such devices depends on the operating temperature and the applied current. Consequently, for additional wavelength tuning *via* temperature the laser was equipped with a Peltier element and a thermoresistive temperature sensor. Fig. 2 shows the corresponding emission characteristics as a function of current and temperature. For a temperature around 25 °C and current in the range of 36–45 mA, the DFB-QCL enables mode-hop-free spectral tuning from 3.367 μm to 3.370 μm. Furthermore, the

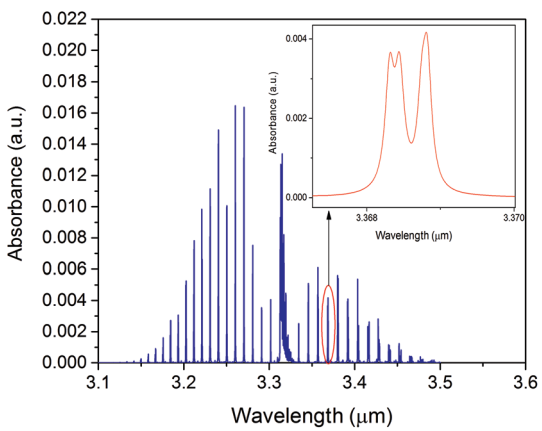

Fig. 1 Absorbance spectrum of methane (100 ppm_v) at ambient conditions and the zoomed area relative to the region 3.363–3.370 μm.

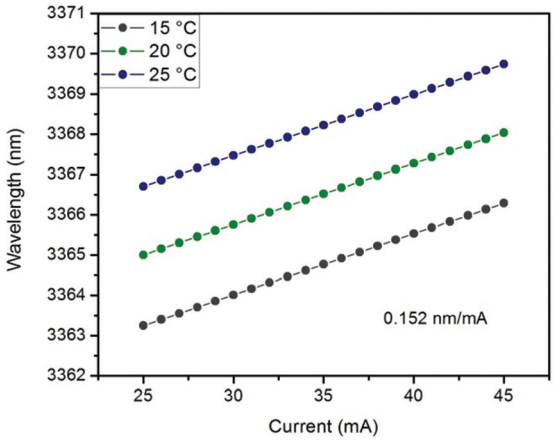

Fig. 2 Tuning of the DFB-ICL emission wavelength as a function of the applied current and temperature.

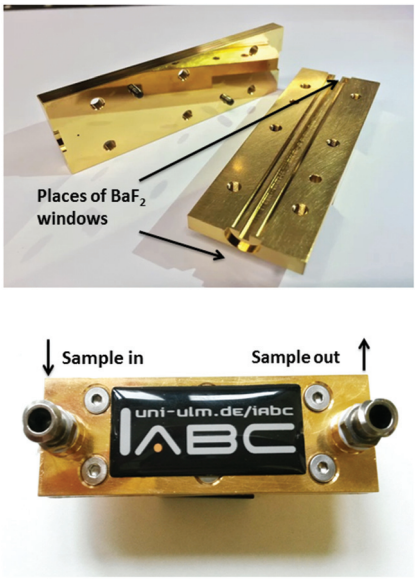

Fig. 3 Optical image of the gold coated brass ($CuZn_x$) iHWG. The wave-guiding channel propagating photons is sealed with MIR-transparent BaF_2 windows (not visible), and gas samples are simultaneously flown through the iHWG channel *via* the gas in/out ports providing access through the top substrate of the channel.

device exhibits wavelength tuning rates of 0.152 nm mA^{-1} and approx. 0.3 nm $°C^{-1}$.[20] The slope efficiency is approx. 0.41 mW mA^{-1}, and the maximum optical output power equals 4.8 mW.

Substrate-integrated hollow waveguide

Substrate-integrated hollow waveguides (iHWG) are a new generation of hollow waveguides recently introduced by the research team of Mizaikoff and collaborators.[18,23–28] Compact dimensions (here, 75 × 25 × 12 mm), tailorability in optical (*i.e.*, hollow waveguide channel) design, flexibility in the substrate material, and minimal volume of gas sample required for analysis (few hundred microliters) resulting in particularly short sample transient times evidence the main advantages of iHWGs next to their robustness and cost-effectiveness. Here, a gold-coated brass ($CuZn_x$) iHWG (Fig. 3) providing an integrated hollow waveguide channel length of 7.5 cm was used.

Experimental setup

The experimental sensor setup for methane analysis is schematically shown in Fig. 4. A DFB-ICL (Nanoplus GmbH) mounted on a TO66 header operated in CW-mode emitting single-mode MIR radiation centered at 3.366 μm was used as the light source (A). The TO66 header was enclosed in a 5 cm^3 heat sink assembly combined with a thermoelectric cooler driver unit (B). The laser injection current control was enabled *via* an appropriate laser driver (C). A waveform generator provided a triangular ramp at 200 Hz (D). The laser temperature was kept constant during the measurement, and wavelength tuning was realized *via* direct modulation of the injection current. The laser was collimated *via* gold-coated off-axis parabolic mirrors (E) with a focal length of $f(L)$ = 50.8 mm (2″), and focused into the waveguide channel of the iHWG (nominal optical path: 7.5 cm, waveguide/gas cell channel dimensions: 2 × 2 mm) (F). The exiting laser beam was again collimated *via* an off-axis parabolic mirror, and focused onto a

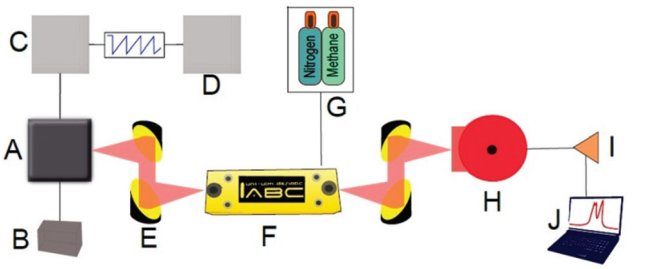

Fig. 4 Experimental sensor setup. (A) DFB-ICL laser, (B) temperature controller, (C) laser controller, (D) function generator, (E) gold-coated off-axis parabolic mirrors, (F) gold-coated brass iHWG, (G) gas mixing system (GMS), (H) MCT-detector, (I) lock-in amplifier, and (J) computer for data analysis.

liquid nitrogen cooled mercury–cadmium–telluride (MCT) detector (Infrared Associates, USA) (H) connected to a lock-in amplifier (I). A gas mixing system (GMS, developed in collaboration with LLNL-Lawrence Livermore National Laboratory, Livermore, USA) (G) provides the carrier gas (N_2) and the methane samples during the measurements.

Spectra were collected using an oscilloscope. The 200 Hz saw-tooth-wave with an offset of 1.2 V and a peak-to-peak amplitude of 2 V was sent to the ramp input of the ICL driver system, thereby resulting in an ICL current scan from 36.0–44.0 mA. This current range – as previously mentioned – corresponds to a wavelength coverage from 3.367–3.370 μm. Synchronously, the spectral data from the MCT-detector is recorded at a sampling rate of 10 kS s^{-1}.

Results and discussion

Selection of the optimum target absorption line is a key aspect in MIR gas phase sensing. The methane line located between 3.367 and 3.370 μm, which is free from interferences with other atmospheric constituents was therefore ideally suited providing an intensity of approx. 2.0×10^{-18} cm per molecule.[21]

A typical sensor signal for methane (exemplarily 2000 ppm_v in nitrogen) and a corresponding background signal (N_2) are depicted in Fig. 5. Prior to any methane measurement, the sensor was purged with pure nitrogen for 5 min at a flow rate of 200 mL min^{-1} ensuring that any residual methane is removed from the tubing; in addition, the iHWG was purged for 3 min. Here, it is noteworthy that iHWG before purging provided a peak-to-peak signal around 1.8–1.9 V, which increased to 2 V after purging. Hence, 90–95% of optical power was collected at the distal output of the iHWG.

The methane spectrum was obtained using a three-step algorithm. In the first step, 200 spectral sweeps were averaged, and the absorption peak was obtained by calculating the absorbance using the following equation:

$$A = -\log(I - \text{offset}/I_0 - \text{offset}) \quad (1)$$

where A represents the absorbance, I is the intensity, I_0 is the reference, and offset is the signal intensity once the laser was turned off (*i.e.*, blank signal). In the second step, the sloping baseline of the spectral scan was using a 2nd derivative with adjacent-averaging smoothing. Finally, a Voigt line shape was fitted to the absorption peaks, and the third peak fitted (singlet) was used to establish analytical calibration functions (OriginPro 2015 software package; OriginLab Corporation, USA).

The Voigt fit is a peak fitting technique that involves a combination of Fourier spectral and profile modeling. This technique can be applied for UV spectral analysis, for chromatograms, and for infrared spectra recorded *via* Fourier transform infrared (FT-IR) spectroscopy. For IR spectra, it is evident that a Voigt fit is superior to a Gauss or Lorentz profile, and leads to a more accurate and descriptive peak facilitating quantification.[29]

Fig. 6 shows the resulting absorbance spectra of methane at different concentrations (in N_2), and the analytical calibration function for the investigated concentration range. The position of the absorption lines and the obtained line widths are in excellent agreement with the corresponding calculated spectra derived *via* the HITRAN database (*i.e.*, amplitude ratio of the lines shows a max 8–15% variance when compared to the HITRAN spectrum).

An analytical calibration function based on the evaluation of the peak height after Voigt fit *vs.* the CH_4 concentrations was established for quantitative data evaluation. For each concentration, twelve measurements were performed, and each spectrum was calculated as the average of two sets of six measurements. Table 1 summarizes the analytical figures-of-merit obtained with the iHWG sensor. The developed method revealed excellent linearity over the concentration range of 100–2000 ppm_v for CH_4 (r^2 = 0.9999). The limit of detection (LoD) considered as three times the standard deviation of the

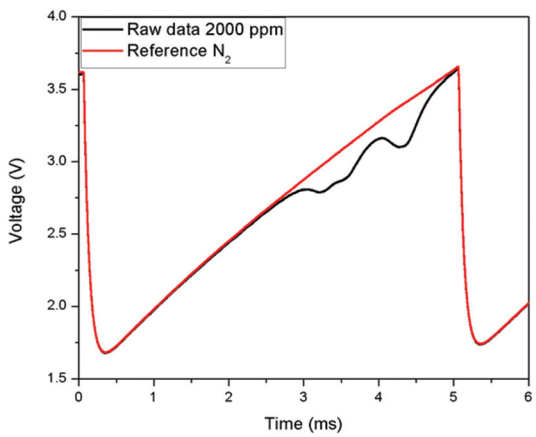

Fig. 5 Interference-free absorption line of CH_4 in the range 3.367–3.370 μm *vs.* background (N_2).

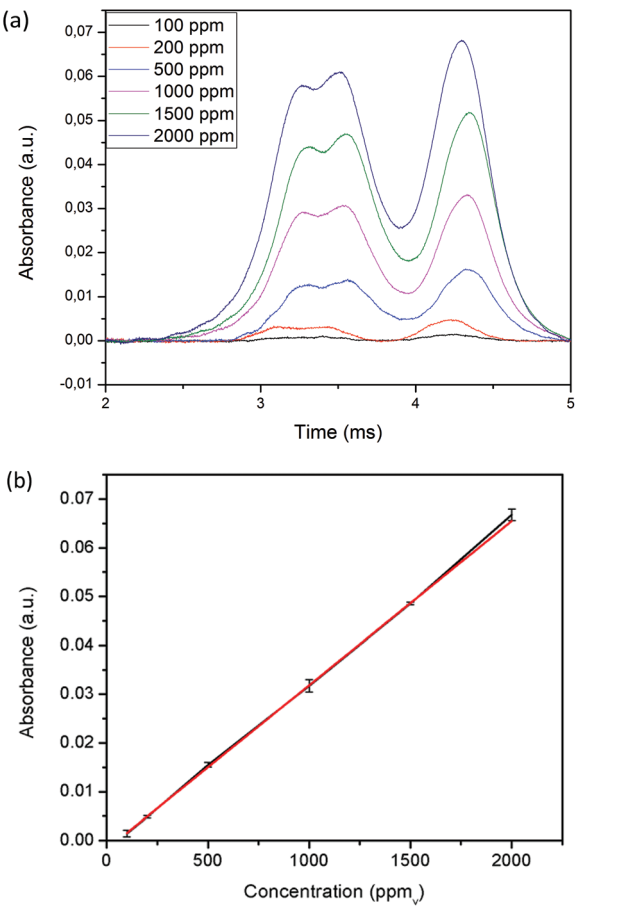

Fig. 6 (a) Exemplary absorbance spectra of methane (100–2000 ppm_v); (b) calibration function for methane (100–2000 ppm_v).

Table 1 Analytical figures-of-merit obtained for the ICL-iHWG methane sensor

Parameter	Value
Limit of detection (3 × SD of blank)/slope	38.0 ± 0.7 ppm_v
Limit of quantification (10 × SD of blank)/slope	127.0 ± 0.7 ppm_v
Correlation coefficient	0.9999
Linear range	100–2000 ppm_v
Regression equation	$A = 3.36455 \times 10^{-5}\,[CH_4] - 0.0018$
Signal-to-noise ratio (@2000 ppm_v)	74

blank signal, was determined as 38 ppm_v with a standard deviation of 0.7 ppm_v.

The robustness of the ICL-iHWG methane sensor was investigated by applying the Allan variance (a.k.a., Allan–Werle variance), *i.e.*, a metric nowadays commonly used to quantify precision and stability of laser-based analyzers.[30,31] Fig. 7 shows the Allan variance graph obtained from the continuous measurements of methane gas at 500 ppm_v over extended periods of time.

The first data point indicates a precision level of approx. 0.62 ppb_v. The corresponding Allan analysis revealed that the sensor facilitates an averaging time of up to 256 s, with a corresponding optimum precision for CH_4 at approx. 0.062 ppb_v after 4 min of signal averaging. The slope of the solid fit line gives the theoretical behavior (*i.e.*, expected $1/\tau$) for a system dominated by white noise. For integration periods smaller than $\tau_{optimum}$, the increase in integration time leads to a decrease in variance, as anticipated by following the theoretical slope. However, the variance increase for extended integration times (*i.e.*, beyond $\tau_{optimum}$), as any kind of environmental parameter such as vibrations, temperature and pressure changes, *etc*. will detrimentally affect the overall system noise. The rather outstanding sensitivity and exceptional measurement precision illustrate the high performance of the developed ICL-iHWG methane sensor system.

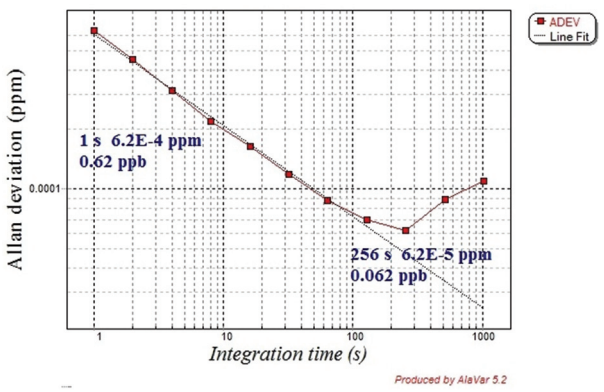

Fig. 7 Allan variance derived from measurements of CH_4 using the ICL-iHWG sensor system over extended periods of time. The Allan variance analysis reveals a minimum level of noise (*i.e.*, 0.062 ppb_v) for an integration period of 256 s.

Hence, it is anticipated that even at in-field conditions and with substantially more influencing parameters the system stability and robustness enable accurate measurements at relevant concentration levels.

Conclusions

In this study, we described the first combination of a new generation of hollow waveguides, *i.e.*, substrate-integrated hollow waveguides (iHWGs) with tunable interband cascade lasers (ICLs) for sensing methane. Our results indicate that the measurement precision of the sensor is 0.62 ppb_v for a 1 s averaging time, and can be maximized at 0.062 ppb_v with a 250 s integration time. The limit of detection for this device has been determined at 38 ppm_v, thereby rendering the sensor useful for emission monitoring and process control applications.

Finally, it should be noted that the sensor developed in this study is a prototype, and not yet fully optimized. In particular, the optical path length for further decreasing the LoD, the thermal (and thus temporal) stability of iHWG, as well as the dependence on additional environmental factors such as relative humidity will be the subject of future investigations.

Acknowledgements

Support for this study by the project APOSEMA funded by the German BMBF/VDI within the M-Era.net program is greatly acknowledged. This work was also supported by CNPq (Project 407170/2013-8; OSTEMPA-Optical Sensor Technologies for Environmental, Medical, and Process Analytics), and INCTAA (CNPq 573894/2008-6 and FAPESP 2008/57808-1). The Machine Shop at Ulm University is thanked for assistance during prototype development of the iHWG. This work was performed in part under the auspices of the U.S. Department of Energy by Lawrence Livermore National Laboratory (LLNL) under Contract DE-AC52-07NA27344.

References

1 J. J. West, A. M. Fiore, L. W. Horowitz and D. L. Mauzerall, *Proc. Natl. Acad. Sci. U. S. A.*, 2006, **103**, 3988–3993.
2 C. Hovde, D. B. Oh, M. A. Zondlo, C. Soo Kim, M. Kim, W. Bewley, C. L. Canedy, I. Vurgaftman, J. R. Meyer, S. G. Jones, T. A. R. Schmidt and K. M. Suzuki, in *Proc. of SPIE*, ed. K. J. Ewing, J. B. Gillespie, P. M. Chu and W. J. Marinelli, 2007, vol. 6756, p. 67560B.
3 J. Jo, Y. S. Kwon, J. W. Lee, J. S. Park, B. H. Rho and W. Choi, *Respir. Dis.*, 2013, **74**(3), 120–123.
4 C. Fischer and M. W. Sigrist, *Appl. Phys. B: Lasers Opt.*, 2002, **75**, 305–310.
5 D. Kleine, H. Dahnke, W. Urban, P. Hering and M. Mürtz, *Opt. Lett.*, 2000, **25**, 1606–1608.
6 Q. Tan, L. Tang, M. Yang, C. Xue, W. Zhang, J. Liu and J. Xiong, *Opt. Lasers Eng.*, 2015, **74**, 103–108.

7 K. Liu, L. Wang, T. Tan, G. Wang, W. Zhang, W. Chen and X. Gao, *Sens. Actuators, B*, 2015, **220**, 1000–1005.
8 G. Bekiaris, J. M. Triolo, C. Peltre, L. Pedersen, L. S. Jensen and S. Bruun, *Bioresour. Technol.*, 2015, **197**, 475–481.
9 M. Rahimi, I. Chae, J. E. Hawk, S. K. Mitra and T. Thundat, *Sens. Actuators, B*, 2015, **221**, 564–569.
10 P. Geiser, *Sensors*, 2015, **15**, 22724–22736.
11 C. S. Kim, M. Kim, W. W. Bewley, J. R. Lindle, C. L. Canedy, J. Abell, I. Vurgaftman and J. R. Meyer, *Appl. Phys. Lett.*, 2009, **95**, 231103.
12 T. R. Tsai, I. Trofimov, C. W. Heaps, M. Maiorov, V. Zeidel, C. S. Kim, M. Kim, C. L. Canedy, W. W. Bewley, J. R. Lindle, I. Vurgaftman, J. Meyer and G. Wysocki, Conf. Lasers Electro-Optics 2010, 2010, CThM4.
13 J. H. N. Orthern, S. O. H. Agan, B. F. Letcher, B. G. Ras, P. E. Wart, C. S. K. Im, M. K. Im, C. D. M. Erritt, W. W. B. Ewley, C. L. C. Anedy, J. A. Bell, I. V. Urgaftman and J. R. M. Eyer, *Opt. Lett.*, 2015, **40**, 4186–4189.
14 J. J. Scherer, J. B. Paul, H. J. Jost and M. L. Fischer, *Appl. Phys. B*, 2012, **110**, 271–277.
15 G. Hancock, J. H. van Helden, R. Peverall, G. A. D. Ritchie and R. J. Walker, *Appl. Phys. Lett.*, 2009, **94**, 201110.
16 L. Naehle, S. Belahsene, M. von Edlinger, M. Fischer, G. Boissier, P. Grech, G. Narcy, A. Vicet, Y. Rouillard, J. Koeth and L. Worschech, *Electron. Lett.*, 2011, **47**, 46.
17 I. Vurgaftman, R. Weih, M. Kamp, J. R. Meyer, C. L. Canedy, C. S. Kim, M. Kim, W. W. Bewley, C. D. Merritt, J. Abell and S. Höfling, *J. Phys. D: Appl. Phys.*, 2015, **48**, 123001.
18 A. Wilk, J. C. Carter, M. Chrisp, A. M. Manuel, P. Mirkarimi, J. B. Alameda and B. Mizaikoff, *Anal. Chem.*, 2013, **85**, 11205–11210.
19 J. Cao, K. Zhang, Z. Wang, R. Yang and Y. Wang, 2010 Symp. Photonics Optoelectron., 2010, pp. 1–5.
20 M. Wolff, S. Rhein, H. Bruhns, L. Nähle, M. Fischer and J. Koeth, *Sens. Actuators, B*, 2013, **187**, 574–577.
21 L. S. Rothman, I. E. Gordon, Y. Babikov, A. Barbe, D. Chris Benner, P. F. Bernath, M. Birk, L. Bizzocchi, V. Boudon, L. R. Brown, A. Campargue, K. Chance, E. A. Cohen, L. H. Coudert, V. M. Devi, B. J. Drouin, A. Fayt, J. M. Flaud, R. R. Gamache, J. J. Harrison, J. M. Hartmann, C. Hill, J. T. Hodges, D. Jacquemart, A. Jolly, J. Lamouroux, R. J. Le Roy, G. Li, D. A. Long, O. M. Lyulin, C. J. Mackie, S. T. Massie, S. Mikhailenko, H. S. P. Müller, O. V. Naumenko, A. V. Nikitin, J. Orphal, V. Perevalov, A. Perrin, E. R. Polovtseva, C. Richard, M. A. H. Smith, E. Starikova, K. Sung, S. Tashkun, J. Tennyson, G. C. Toon, V. G. Tyuterev and G. Wagner, *J. Quant. Spectrosc. Radiat. Transfer*, 2013, **130**, 4–50.
22 J. M. Wolf, A. Bismuto, M. Beck and J. Faist, *Opt. Express*, 2014, **22**, 2111.
23 J. J. R. Rohwedder, C. Pasquini, P. R. Fortes, I. M. Raimundo, A. Wilk and B. Mizaikoff, *Analyst*, 2014, **139**, 3572–3576.
24 V. Kokoric, A. Wilk and B. Mizaikoff, *Anal. Methods*, 2015, **7**, 3664–3667.
25 J. F. D. S. Petruci, P. R. Fortes, V. Kokoric, A. Wilk, I. M. Raimundo, A. A. Cardoso and B. Mizaikoff, *Analyst*, 2014, **139**, 198–203.
26 J. F. D. S. Petruci, A. A. Cardoso, A. Wilk, V. Kokoric and B. Mizaikoff, *Anal. Chem.*, 2015, **87**, 9580–9583.
27 J. F. da Silveira Petruci, P. R. Fortes, V. Kokoric, A. Wilk, I. M. Raimundo, A. A. Cardoso and B. Mizaikoff, *Sci. Rep.*, 2013, **3**, 3174.
28 J. F. D. S. Petruci, A. Wilk, A. A. Cardoso and B. Mizaikoff, *Anal. Chem.*, 2015, 150924110051003.
29 J. T. Reilly, J. M. Walsh, M. L. Greenfield and M. D. Donohue, *Spectrochim. Acta, Part A*, 1992, **48**, 1459–1479.
30 P. Werle, *Appl. Phys. B*, 2011, **102**, 313–329.
31 P. Werle, R. Mücke and F. Slemr, *Appl. Phys. B*, 1993, **57**, 131–139.